Materials Today Energy 45 (2024) 101673

Contents lists available at ScienceDirect

Materials Today Energy

journal homepage: www.journals.elsevier.com/materials-today-energy/

Green-light wavelength-selective organic solar cells: module fabrication and crop evaluation towards agrivoltaics

Shreyam Chatterjee [a, **], Naoto Shimohara [a], Takuji Seo [a], Seihou Jinnai [a, b], Taichi Moriyama [c], Morihiko Saida [d], Kenji Omote [d], Kento Hama [e], Yohei Iimuro [e], Yasuyuki Watanabe [e, ***], Yutaka Ie [a, b, *]

[a] The Institute of Scientific and Industrial Research (SANKEN), Osaka University, 8-1, Mihogaoka, Ibaraki, Osaka 567-0047, Japan
[b] Innovative Catalysis Science Division, Institute for Open and Transdisciplinary Research Initiatives (OTRI), Osaka University, 2-1 Yamadaoka, Suita, Osaka 565-0871, Japan
[c] Ishihara Sangyo Kaisha, Ltd., 3-1 Nishi-shibukawa 2-chome, Kusatsu, Shiga 525-0025, Japan
[d] Designsolar Co. Ltd., LABO CITY SENDAI, 6-6-3, Minamiyoshinari, Aoba-ku, Sendai, 989-3204, Japan
[e] Department of Mechanical and Electrical Engineering, Faculty of Engineering, Suwa University of Science, 5000-1 Toyohira, Chino, Nagano 391-0292, Japan

ARTICLE INFO

Article history:
Received 2 August 2024
Received in revised form
12 August 2024
Accepted 13 August 2024
Available online 20 August 2024

Keywords:
Non-fullerene acceptors
poly(3-hexylthiophene)
Organic photovoltaics
Greenhouse technology
Fluorinated-naphthobisthiadiazole
Agriphotovoltaics

ABSTRACT

Green-light wavelength-selective organic solar cells (GLWS-OSCs) pioneer novel agrivoltaics in greenhouses via transforming solar energy in the green-light region to electricity while simultaneously growing crops by utilizing the transmitted blue and red lights. However, the development of GLWS-OSCs has been stymied due to the limited availability of donors and acceptors. Herein, we investigate the combination of a cost-effective poly(3-hexylthiophene) (P3HT) donor with a fluorinated-naphthobisthiadiazole-based non-fullerene acceptor (FNTz-FA) for GLWS-OSC application. FNTz-FA shows an intense absorption band between 500 and 600 nm and a high level of chemical stability. OSCs based on P3HT and FNTz-FA with an inverted configuration are optimized to show high green-light wavelength-selective absorption and power conversion efficiency in the green-light region. Furthermore, large-scale device fabrication has been considered, leading to the development of 100 and 400 cm^2 scale OSC modules. These modules showed sustained solar cell performance after 180 days. Photosynthetic rate measurements indicate that transmissions by the P3HT:FNTz-FA film show a non-obstructing nature and the advantage of green-light wavelength-selectivity in crop growth. Preliminary investigations on the growth of tomatoes have shown the potential of P3HT:FNTz-FA-based OSCs for agrivoltaics. These results demonstrate that GLWS-OSCs are a valid candidate to realize agrivoltaics in greenhouses for an effective utilization of solar energy.

1. Introduction

The energy sources for electricity in agriculture largely rely on fossil fuels such as heavy oil. Therefore, solar cells are expected to be a promising innovative technology that could reduce the greenhouse gas emissions caused by the release of carbon dioxide [1,2]. In this context, the use of silicon solar cells in agriculture, which is referred to as a solar-sharing system, is gaining popularity particularly for large-scale agricultural operations [3,4]. Greenhouses have been extensively utilized as a protected form of horticulture that realizes the effective operation of agricultural land by controlling several cultivation environments such as intensity of solar radiation, temperature, humidity, and CO_2 concentration, all of which are crucial in maximizing the best qualities of crop growth. Although electricity is indispensable for greenhouses to maintain optimal crop-growing conditions, the installation of silicon solar cells on the roofs of greenhouses faces the critical problem of low-transmittance properties that decrease crop yields. Furthermore, the heavy weight and inflexibility of silicon solar cells necessitates the use of mounting structures, which is also a

* Corresponding author.
** Corresponding author.
*** Corresponding author.
E-mail addresses: shreyam@sanken.osaka-u.ac.jp (S. Chatterjee), watanbey@rs.sus.ac.jp (Y. Watanabe), yutakaie@sanken.osaka-u.ac.jp (Y. Ie).

https://doi.org/10.1016/j.mtener.2024.101673

drawback for greenhouse applications. Perovskite solar cells, which are positioned as next-generation solar cells, are not suitable for greenhouse applications due to the use of toxic lead components in the active layer [5,6].

Organic solar cells (OSCs) have been extensively investigated in recent years as a next-generation energy source due to their distinct features such as light weight, flexibility, solution processability, and cost effectiveness [7]. The active layer of OSCs is composed of two types of organic semiconductors, hole-transporting materials (donors) and electron-transporting materials (acceptors), the absorption properties of which could be finely tuned by adjusting the optical band gaps (E_gs). Photosynthetically active pigments of chlorophyll a and b in the plants are well known to have absorption bands in the blue and red wavelength regions (Fig. 1a). The carotenoid pigments also show similar absorption characteristics [8]. Thus, effective utilization of the optical window of the green-light wavelength region via adjustment of the E_gs of donors (E_g(D)) and acceptors (E_g(A)) to the same levels has allowed the development of a solar cell system that simultaneously harvests solar energy to produce the electricity needed to maintain an environment suitable for crop growth (Fig. 1b) [9]. It should be mentioned that the concept of the wavelength-selective utilization of solar light in our OSCs is different from that of conventional agrivoltaics based on transmitted semitransparent OSCs [10–17] because the most critical factor for agrivoltaics in greenhouse is achieving sufficient crop yield.

By applying the advantages of OSCs to this hypothesis, we recently proposed green-light wavelength-selective (GLWS) OSCs based on poly(3-hexylthiophene) (P3HT) as a donor and an electron-accepting π-conjugated compound (SNTz-RD) as a non-fullerene acceptor (NFA) (Fig. 1c) [9]. It should be emphasized here that we selected P3HT as the donor due to the advantages of green-light wavelength-selective absorption (Fig. 1a) and bulk availability at a low cost [18–24]. Thus, overlapping the absorption spectrum of NFA with that of P3HT is one of the prime criteria for realizing GLWS-OSCs (Fig. 1b). In fact, the P3HT:SNTz-RD film showed a green-light wavelength-selective factor (S_G) of 0.44 and a moderate power conversion efficiency of 5.8% in the green-light region (PCE-GR) (see Material and methods section for details of S_G) [9]. We also recently investigated the influence that the green-light wavelength-variation of NFAs exerts on the photosynthetic rate, and an NFA based on electron-accepting π-conjugated molecules bearing cyclopentene-annelated thiophene with a spiro-substituted 2,7-bis(2-ethylhexyl)fluorene unit improved the S_G to 0.52 and the PCE-GR to 7.8% when combined with P3HT [25]. However, further improvement in both the S_G and the PCE-GR would be indispensable for the social implementation of GLWS-OSCs.

As an NFA candidate that satisfies these criteria, we focused on a fluorinated naphtho[1,2-*c*:5,6-*c*']bis[1,2,5]thiadiazole (FNTz)-based compound (FNTz-FA) (Fig. 1c) because this molecule exhibits a high level of green-light wavelength-selective absorption and better photovoltaic characteristics when combined with P3HT [26,27]. For this application, we investigated the physicochemical properties, OSC optimization for a module, the photosynthetic rate, and preliminarily evaluated crop growth.

2. Materials and methods

2.1. Materials and property measurements

The synthesis of FNTz-FA and its complete characterization can be found in previously published work [26,27]. P3HT was purchased from Sigma Aldrich. UV–vis spectra were recorded on a Shimadzu UV-3600 spectrophotometer. Low-energy inverse photoemission spectroscopy (LEIPS) was performed using the Ulvac-Phi, Inc. LEIPS system. The surface structures of the deposited organic films were observed by atomic force microscopy (AFM) (Shimadzu, SPM9600). ToF-SIMS spectra measurements were performed with an M6 device (IONTOF, Münster, Germany). To ensure the sensitivity for sulfur, nitrogen, and fluorine atoms, we utilized negative polarity conditions.

2.2. Determination of S_G

The S_G was determined using the following equation:

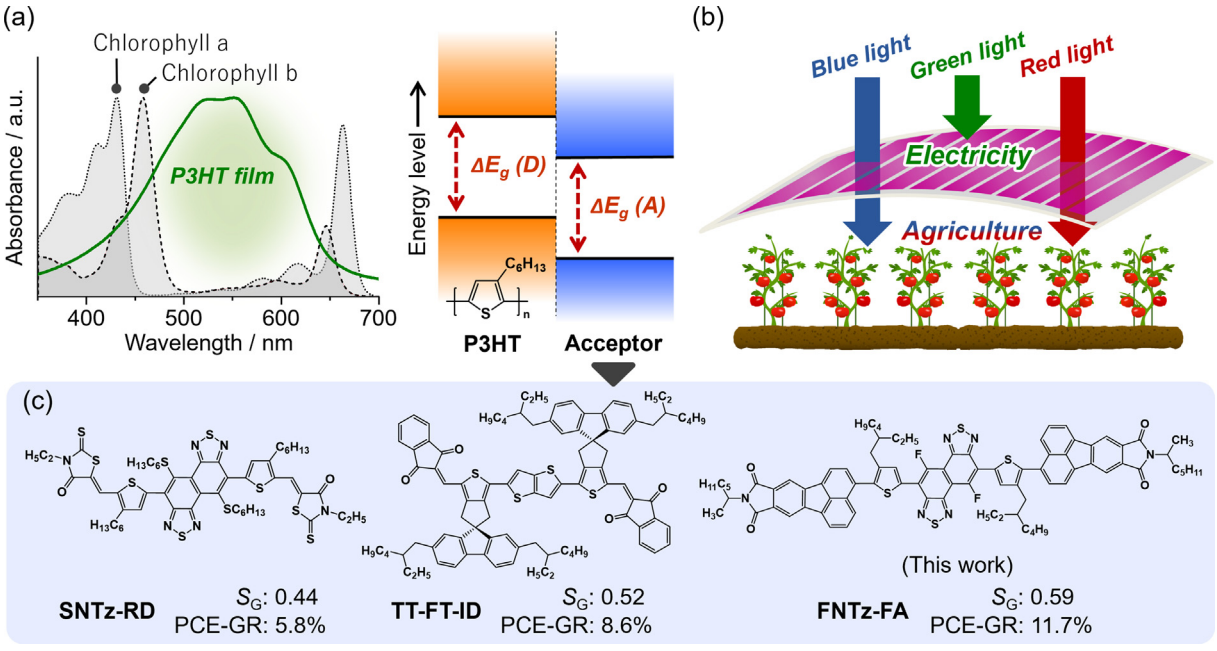

Fig. 1. (a) Absorption spectra of chlorophylls a and b, (b) Schematic image of GLWS-OSCs, and (c) Chemical structures of P3HT and NFAs for GLWS-OSCs.

$$S_G = \left\{ \frac{1}{N_G} \sum_{\lambda \in G} (1 - T) - \frac{1}{N_{RB}} \sum_{\lambda \in RB} (1 - T) \right\} \Big/ \left\{ \frac{1}{N} \sum_{\lambda \in RGB} (1 - T) \right\}$$

where T is the transmittance of the blend film and N_G, N_{RB}, and N are the normalization factors, i.e., the data numbers in the green-light wavelength region (500–600 nm), the blue-and red- wavelength regions (400–500 and 600–700 nm), and the total wavelength region (400–700 nm), respectively. Based on this equation, the S_G value becomes zero when the transmittance spectrum between 400 and 700 nm is completely flat (no selectivity), whereas it approaches 1 when the contribution of the transmittance in the blue and red wavelength regions are increased. On the other hand, the S_G value becomes −1 in the case of wavelength-selective transmittance in the green wavelength region.

2.3. OSC device fabrication and evaluation

OSC devices with a structure of ITO/ZnO/P3HT:acceptor/MoO_3/Ag were prepared. ITO-coated glass substrates were sonicated in acetone, water, and 2-propanol for 10 min, respectively. The resulting ITO-coated glass substrates were then treated with O_3 for 30 min. A ZnO solution of zinc acetate dihydrate (99.9%, 200 mg), ethanolamine (99%, 55 μL), and 2-methoxyethanol (99.8%, 2 mL) was spin-coated onto the substrate at 3500 rpm, which then were baked at 200 °C for 30 min in an ambient atmosphere. The active layer (P3HT:FNTz-FA= 1:1 wt(%), 12 mg/mL or 25 mg/mL in chlorobenzene) was then formed on the ITO/ZnO electrode by spin-coating at 1000 rpm for 120 s. Thermal annealing was performed at 140 °C for 10 min MoO_3 and Ag electrodes were evaporated on the top of the active layer through a shadow mask to define the active area of the devices (0.09 cm^2) under a high vacuum of 10^{-5} Pa to a thickness of 10, 100 nm as determined by a quartz crystal monitor. After sealing the device from the air, the photovoltaic characteristics were measured in air under simulated AM 1.5G solar irradiation (100 mW/cm^2) (SAN-EI ELECTRIC, XES-301S). The J–V characteristics of the photovoltaic devices were measured using a KEITHLEY 2400 source meter. The external quantum efficiency (EQE) spectra were measured using a Soma Optics Ltd. S-9240.

2.4. Module fabrication

The OSC modules on a 100 cm^2 scale were fabricated with an inverted configuration of glass/ITO/AZO/PEI/P3HT:FNTz-FA (1:1 wt(%), 36 mg/mL)/PEDOT:PSS/Au. The AZO and PEI layers were formed by spin-coating at 2000 rpm for 60 s with drying at 105 °C for 5 and 15 min, respectively. The solution process of this fabrication was performed under air-exposed conditions with spin-coating at 1000 rpm for 120 s, followed by thermal annealing at 140 °C for 15 min. A PEDOT:PSS layer was formed by spin-coating at 2000 rpm for 180 s. The thickness of the Au electrodes was approximately 50–100 nm. These OSC devices were sealed by gas-barriered films with a water vapor transmission rate on the order of 10^{-3} g/m^2/day and a total transmittance of 91%. The geometrical fill factor of the module is 0.90.

The OSC modules on a 400 cm^2 scale were fabricated with an inverted configuration of ITO/ZnO-NP/PEI/P3HT:FNTz-FA (1:1 wt(%), 20 mg/mL)/PEDOT:PSS/Ag-paste on PEN substrates. The ZnO-NP, PEI, and P3HT:FNTz-FA layers were formed by blade-coating. A PEDOT:PSS layer was formed by bar-coating. The top Ag electrodes were fabricated by screen printing to achieve a thickness of approximately 10 μm. The geometrical fill factor of the module is 0.89.

2.5. Photosynthesis evaluation

Photosynthetic rates were determined by gas exchange experiments using an Li-6800 photosynthesis system and a SOLAX series XC-100EF light source (SERIC Ltd., Japan). The light saturation point and photosynthetic rate were evaluated at a controlled temperature of 25 °C and a CO_2 concentration of 400 ppm.

3. Results and discussion

3.1. Photophysics of FNTz-FA

The UV–vis absorption spectra of FNTz-FA along with our previous green-light wavelength-selective acceptor SNTz-RD in pristine films are shown in Fig. 2. SNTz-RD showed two absorption bands at around 400–450 and 500–600 nm, and determined that the relatively large molar extinction coefficient of the former band originated from the non-planar π-conjugated framework of SNTz-RD [9,28]. On the other hand, with respect to the relatively planar structure, the FNTz-FA film shows one intense absorption between 500 and 600 nm, which completely covers the green-light region in the visible spectrum. It should be mentioned that the complementary absorption of FNTz-FA against chlorophylls a and b is compatible for agrivoltaics applications (Fig. 2a). The molar extinction coefficient (ε) of FNTz-FA (6.3×10^4 M/cm) is almost 1.5-fold higher than that of SNTz-RD (4.2×10^4 M/cm), which demonstrates the improved photo absorption characteristics of FNTz-FA in solution. Based on the absorption onset in films, the optical energy gaps (ΔE_{opt}) of FNTz-FA was determined to be 2.08 eV, and this value is similar to that of the P3HT film (1.91 eV). In fact, the P3HT:FNTz-FA-blend film also shows complemental absorption against chlorophylls a and b (Fig. 2a).

The electron affinity of FNTz-FA in film was investigated via low-energy inverse photoemission spectroscopy (LEIPS) measurements (Fig. 2b). Based on the onset of the LEIPS spectra, the electron affinity of FNTz-FA was determined to be 3.55 eV. We previously determined the ionization potential of FNTz-FA to be 6.17 eV [26,27]. These physicochemical results indicate the suitability of FNTz-FA for use in applications to GLWS-OSCs (Fig. 2c).

3.2. Chemical stability of FNTz-FA

For application to agrivoltaics, organic semiconducting materials of both donors and acceptors should have sufficient chemical stability. In this context, P3HT has shown a high level of chemical stability in OSC modules under the combination with fullerene derivatives of $PC_{61}BM$ (CAS Registry No. 160848-22-6), and the chemical structure is shown in Fig. S1 in the Electronic Supplementary Information [29,30]. On the other hand, the chemical stability of NFAs based on electron-accepting π-conjugated systems continues to demonstrate room for improvement. For example, representative NFAs such as ITIC (CAS Registry No. 1664293-06-4) and Y6 (CAS Registry No. 2304444-49-1) contain electrophilic C–C double bonds between the thiophene and the terminal unit, and these double bonds are susceptible to Lewis bases, which decompose the π-conjugated molecular skeleton [31–33]. Since the polyethylenimine/polyethylenimine ethoxylated (PEI/PEIE) version containing amine functional groups has been widely used as an air-stable electron injection layer in the fabrication of OSCs [34,35], 2-aminoethanol (AE) has been adopted as the reagent that should be used to analyze the stability of the NFAs [33]. Therefore, the chemical stability of FNTz-FA in films was investigated via exposure to AE vapor for 30 min (Fig. 3a), after which it was compared with the representative NFAs of ITIC and Y6. The chemical structures of ITIC and Y6 are shown in Fig. S1. As shown in Fig. 3b, the original

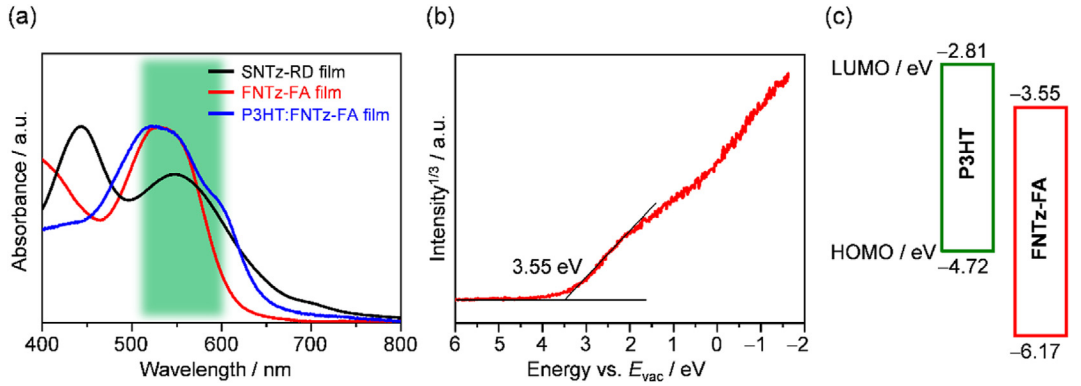

Fig. 2. UV−vis absorption spectra of (a) SNTz-RD (black), FNTz-FA (red), and P3HT:FNTz-FA (blue) in films. (b) LEIPS spectrum of the FNTz-FA film. (c) Energy level diagram of P3HT and non-fullerene acceptors.. LEIPS: low-energy inverse photoemission spectroscopy.

absorption spectra of the ITIC and Y6 films completely disappeared and reappeared as a broad and weak spectrum. These spectral changes are derived from the low chemical stability at the C−C double bonds as the amino groups in AE undergo nucleophilic reactions with the linker C−C double bonds [31,36]. On the other hand, the FNTz-FA films retained the absorption spectrum after exposure to the AE vapor (Fig. 3a). This stability is explained by the inertness of the linking C−C bond between thiophene and terminal FA units.

To further investigate the stability of FNTz-FA under conditions that approximate an actual usage environment, we fabricated the P3HT:FNTz-FA films on transparent polyimide substrates, which were sealed with gas-barriered films. Note that we selected gas-barriered films with a water vapor transmission rate on the order of 10^{-3} g/m^2/day and a total transmittance of ~90%, which is a typical level for OSC applications. After 0, 14, and 24 days, the UV−vis absorption spectra of the P3HT:FNTz-FA films were measured under exposure to sunlight. As shown in Fig. 3c, the absorption spectra of the P3HT:FNTz-FA films were retained even after 24 days. These results clearly indicate that the FNTz-FA possesses sufficient chemical stability for OSC applications.

3.3. Optimization of OSCs for module fabrication

We previously reported that the P3HT:FNTz-FA-based OSCs with the conventional structure of indium tin oxide (ITO)/poly(3,4-ethylenedioxythiophene)-poly(styrenesulfonate) (PEDOT:PSS)/

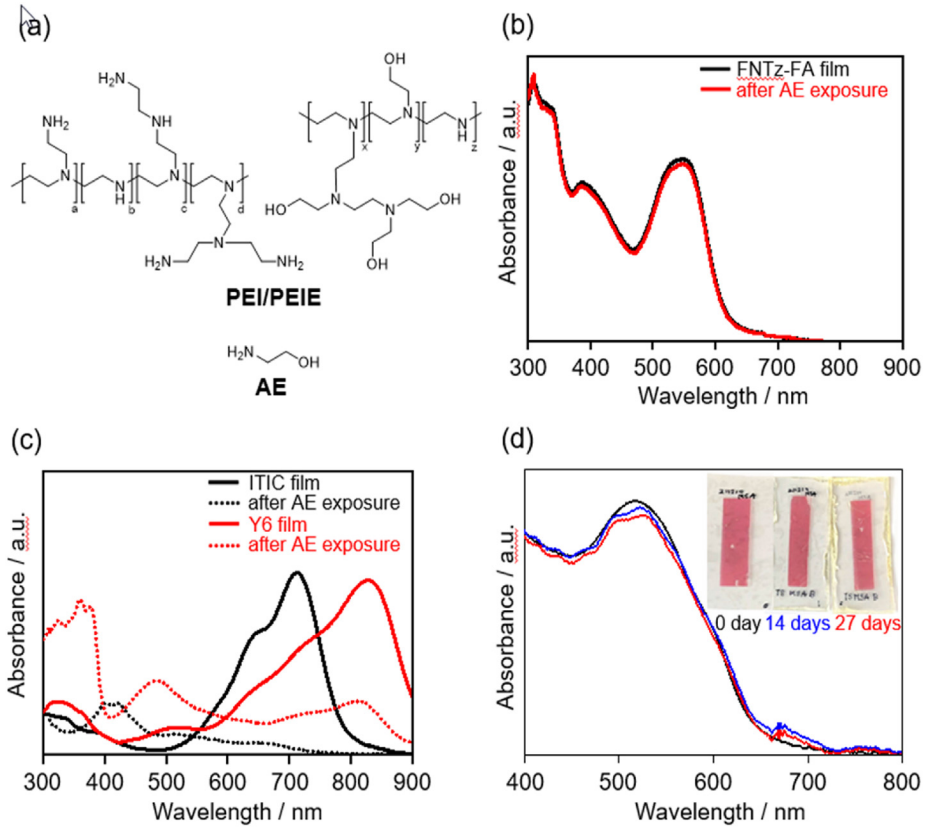

Fig. 3. (a) Chemical structures of PEI/PEIE and AE, UV−vis absorption spectra of (b) FNTz-FA and (c) ITIC and Y6 films before (black line) and after exposure to AE for 30 min (dotted line) (d) Time-dependent UV−vis absorption spectra of the P3HT:FNTz-FA film with a gas barrier following encapsulation.

active layer/Ca/Al showed good photovoltaic characteristics with the highest PCE of 3.12% [26]. The etching of the ITO substrate by the acidic PEDOT:PSS [37,38] and the presence of an easily oxidized low work-function metal electrode containing an upper layer of Ca/Al is often believed to be the main reason for the instability of non-encapsulated conventional OSCs under ambient conditions. The poor environmental stability of the conventional structure of OSCs motivated us to examine the use of an inverted architecture [39]. For the fabrication of large-scale OSCs, PEDOT:PSS is commonly used for the hole-transport layer due to the advantage of the applicability of solution processing based on hydrophilic solvents such as H_2O and EtOH [40–42]. When considering a scale-up of the P3HT:FNTz-FA-based OSCs to module size, we started by optimizing cell-sized devices (0.09 cm^2) with an inverted configuration of glass/ITO/ZnO/P3HT:FNTz-FA/PEDOT:PSS/Ag. Note that the fabrication process after obtaining the active layer was carried out under a nitrogen atmosphere without exposure to air. During optimization of the process solvent, concentration, and the spin-coating conditions, we found that the combination of a low concentration (12 mg/mL) and a low rotation speed of 500 rpm is effective to obtain the best PCE values of 3.02% (Fig. 4a, run 1). The current density (J)–voltage (V) characteristics of the OSCs are shown in Fig. 4a. The typical OSC parameters of a short-circuit current (J_{SC}), an open-circuit voltage (V_{OC}), and a fill factor (FF) are summarized in Table 1, and the detailed optimization reproducibility data are summarized in Figs. S2, S3, S4, S5, S6 and in Tables S1, S2, S3, S4, and S5. This PCE value is tantamount to that obtained from conventional OSCs, and time-of-flight secondary ion mass spectrometry (ToF-SIMS) measurements of this film showed an almost uniform distribution of P3HT and FNTz-FA, irrespective of the depth direction of the thin film (Fig. S7) [43]. Thus, we concluded that the P3HT:FNTz-FA film could be applicable to both conventional and inverted structures. On the other hand, we noticed that these fabrication conditions are ill-suited for the preparation of uniform films in a large-scale module due to the low concentration (6 mg/mL) of P3HT in the ink because the low viscosity that originates from a low concentration created difficulties in achieving homogenous coatings during large-area fabrications via roll-to-roll processing [44]. Thus, we also determined other optimization conditions such as higher-blend concentrations (25 mg/mL) and rotation speeds (1000 rpm), which resulted in a slight decrease in the PCEs of 2.17% (run 2).

To investigate the film morphologies of these blend films, AFM measurements were performed (Fig. 4b). The AFM height images of the P3HT:FNTz-FA-blend films under low concentration conditions (12 mg/mL) (run 1) showed relatively smooth surface morphologies with an average roughness (R_a) of 1.43 nm, compared with that of R_a using high-concentration (25 mg/mL) films (1.58 nm) (run 2). Since these AFM measurements indicate that the relatively smooth morphologies are favorable for the P3HT:FNTz-FA-based OSCs, we considered that the slightly increased R_a value of the high-concentration film could almost be the upper limit that would deliver reasonable device efficiency.

Then, by utilizing the conditions of run 2, we fabricated the OSC modules on a 100 cm^2 scale based on the P3HT:FNTz-FA films (Fig. 4d) with an inverted configuration of glass/ITO/aluminum-doped ZnO nanoparticles (AZO):polyetheleneimine (PEI)/P3HT:FNTz-FA/PEDOT:PSS/Au. It should be mentioned that the solution process of this fabrication was performed under air-exposed conditions. These OSC devices were sealed by gas-barriered films with a water vapor

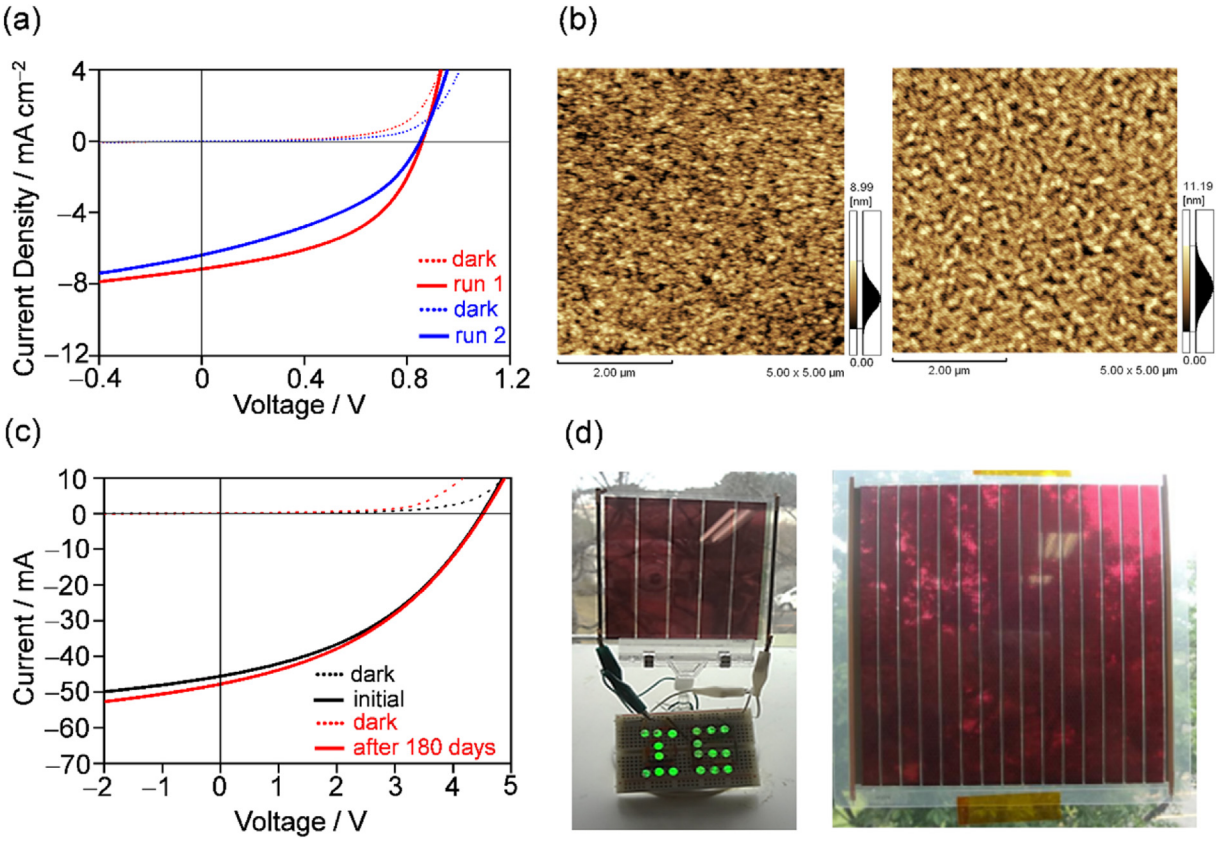

Fig. 4. (a) J–V curves of cell-sized P3HT:FNTz-FA-based OSCs (b) AFM images of P3HT:FNTz-FA-based OSCs fabricated during condition runs 1 (left) and 2 (right) (c) J–V curves of module-size OSCs. (d) Photos of the 100 cm^2-scale (left) and 400 cm^2-scale (right) P3HT:FNTz-FA-based OSCs. modules.

Table 1
OSC characteristics of the cell-sized P3HT:FNTz-FA-based films.

run	J_{SC}/mA/cm^2[a]	V_{OC}/V[a]	FF[a]	PCE/%[a]	PCE-GR/%	S_G
1	7.16 (7.15 ± 0.02)	0.86 (0.86 ± 0.004)	0.49 (0.48 ± 0.004)	3.02 (2.98 ± 0.04)	11.7	0.59
2	6.38 (6.16 ± 0.12)	0.85 (0.85 ± 0.004)	0.40 (0.41 ± 0.006)	2.17 (2.16 ± 0.01)	–	–

[a] Device structure: Glass/ITO/ZnO/P3HT:FNTz-FA/PEDOT:PSS/Ag. The average values and standard deviation of six devices are shown in parentheses.

transmission rate on the order of 10^{-3} g/m^2/day and a total transmittance of 91%. The OSC device showed a moderate PCE value of 1.32% with a J_{SC} of 45.5 mA, a V_{OC} of 4.50 V, and a FF of 0.41 (Fig. 4c). We obtained a similar V_{OC} value (0.90 V) in the module-size device compared with that of a cell-sized device (0.85 V), which indicates that continuous films were formed under the module-size conditions. The scale-up and fabricating conditions influenced a decrease in the PCEs compared with use of the cell-sized device. We decided that the further optimization of fabrication conditions for module-size OSCs improved the PCEs. To investigate the stability of the fabricated OSC modules, we measured the J–V characteristics after 180 days of storage under ambient conditions. As shown in Fig. 4c, almost all the OSC characteristics were retained for the modules with a PCE value of 1.35% (J_{SC}: 47.7 mA, V_{OC}: 4.50 V, and FF: 0.41). These results indicate that the P3HT:FNTz-FA films are applicable to the module-size OSCs for use in agricultural studies. For the crop evaluation, we also prepared the P3HT:FNTz-FA-based OSCs on polyethylene terephthalate substrates with an area of 400 cm^2 (Fig. 4d).

3.4. Green light utilization efficiencies

To determine the green-light utilization efficiencies of the P3HT:FNTz-FA-based OSCs, we measured the EQE spectrum. As shown in Fig. 5a, this device showed wavelength-selective responses between 400 and 600 nm with an EQE maximum of 64% at 513 nm. The estimated J_{SC} calculated from the EQE spectrum was 7.31 mA/cm^2. This value deviates within 2.1% from the observed value, indicating the accuracy of the photovoltaic measurements. This EQE spectrum showed a narrow distribution in the green-wavelength range compared with that of the P3HT:SNTz-RD-based OSCs (Fig. S8) [9]. To quantify the PCE-GR for OSCs, equation (1) was used.

$$\mathrm{PCE-GR} = \left\{ Voc \times \mathrm{FF} \times \sum_{\lambda \epsilon G} (n\mathrm{Photon}_\lambda \times \mathrm{EQE}_\lambda) \right\} \Big/ P_G \times 100\ [\%] \quad (1)$$

In equation (1), EQE_λ and $n\mathrm{Photon}_\lambda$ are the EQEs of the OSCs and the photon flux of AM1.5G at wavelength λ, respectively [9]. In addition, P_G is the irradiated energy in the 500–600 nm wavelength range of AM1.5G (P_G = 15.1 mW/cm^2) [45]. As a result, the PCE-GR of OSCs based on P3HT:FNTz-FA was 11.7%. We also measured the transmittance spectrum of the P3HT:FNTz-FA-blend film. As shown in Fig. 5b, the blend film exhibited a decreased and narrow transmittance in the green-light wavelength region of around 500–600 nm compared with those of the P3HT:SNTz-RD film, but showed a relatively high transmittance in the blue-light and red-light regions. As we expected, this transmittance complements the absorbance of chlorophyll a and chlorophyll b (Fig. S9). The observed transmittance properties of the P3HT:FNTz-FA-blend film is desirable for GLWS-OSCs. A commonly used parameter regarding transmittance in semi-transparent OSCs is the average visible transmission (AVT) [46]. AVT is expressed as a percentage and represents the proportion of visible light that is transmitted through films. Higher AVT values indicate greater transparency or clarity, which allows more light to pass through the film. The AVT of the P3HT:FNTz-FA-blend films was calculated to reach values of 46% [47]. This AVT, however, is not a sufficient parameter for the evaluation of green-light wavelength-selectivity because the total visible regions of blue, green, and red-light wavelengths are taken into consideration. Thus, to evaluate the potential of OSCs for greenhouse applications, we recently proposed the S_G as a quantitative parameter. For example, the representative active layer of a high-performance P3HT-based OSC with O-IDTBR [20] and ZY-4Cl [22] returned S_G values of 0.26 and 0.21, respectively (Fig. S10). Based on this estimation, the S_G value of the P3HT:FNTz-FA-based active layer was calculated to be 0.59, which is higher than that for our previously reported SNTz-RD (0.44). The combined results of PCE-GR and S_G clearly demonstrate the superiority of the green-light wavelength-selectivity of the P3HT:FNTz-FA-blend film over that of the P3HT:SNTz-RD film.

3.5. Crop evaluations

Determining the optimal amount of sunlight irradiation required for the photosynthetic process has been a crucial issue for growing crops using agrivoltaics [48,49]. However, the influence of

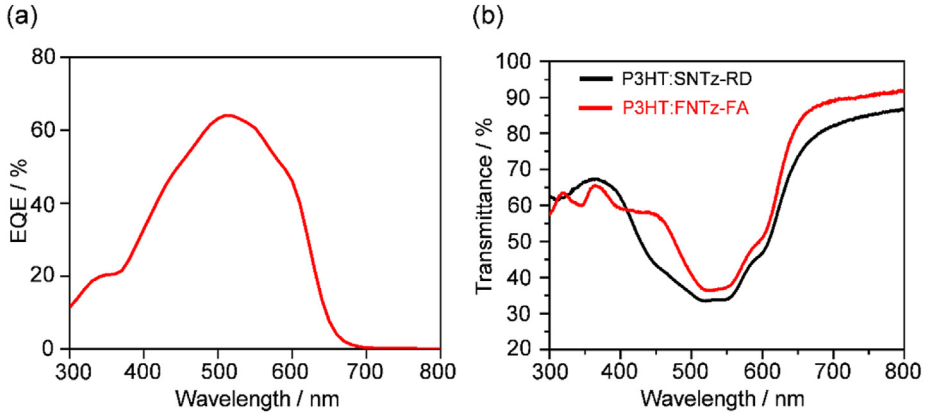

Fig. 5. (a) EQE spectrum of P3HT:FNTz-FA-based OSCs; and, (b) the transmitted spectra of the blend film.

GLWS-OSCs on the photosynthetic process and crop production remains unclear [9]. To reveal the potential of FNTz-FA as NFAs for GLWS-OSCs, we first evaluated the P3HT:FNTz-FA film. Using gas exchange experiments, the photosynthetic rate of strawberry leaves was evaluated under simulated solar irradiation through the P3HT:FNTz-FA films. For this measurement, we fixed the temperature, humidity, and CO_2 concentration in the chamber to be 25 °C, 50%, and 400 ppm, respectively. A photographic image of this experiment is shown in Fig. 6a, and the photosynthetic rate against photosynthetic photon flux density (PPFD) between 0 and 2000 mmol/m^2/s is shown in Fig. 6b. Photosynthetic rates are the average of three measurements taken under each condition. Interestingly, the photosynthetic rates under the transmission of the P3HT:FNTz-FA film almost overlapped that of the control conditions (*i.e.*, using a transparent polyvinyl chloride film). Since both the PPFD at the saturation point of the photosynthetic rate and at the highest photosynthetic rate are almost the same, the influence of the P3HT:FNTz-FA films on the photosynthesis of strawberries is limited.

To examine the contribution of both electricity and crop growth for GLWS-OSCs, we also measured the maximum output power against light intensity for the P3HT:FNTz-FA-based OSCs. As shown in Fig. 6c, the maximum output power increased almost linearly with an increase in the intensity of the solar simulator. The saturation point of the photosynthetic rate in Fig. 6b is around 500 mmol/m^2/s, which corresponds to an irradiance of around 250 W/m^2. Therefore, we inferred that the balanced contribution of electricity and strawberry growth could be accomplished under an irradiance of more than 250 W/m^2.

We next investigated the influence of GLWS-OSCs on the photosynthetic rate. Note that the average transmittance of the P3HT:FNTz-FA-based OSCs is much lower than that of the P3HT:FNTz-FA film because the relatively thicker film of the active layer and the presence of metal electrodes and gas barrier film in the OSCs eventually reduced the average transmittance of the solar light to 22%. A photographic image of this experiment is shown in Fig. 6d. We decided to utilize tomato leaves for this evaluation because tomatoes are a representative crop for greenhouse growth as they require a higher level of solar irradiation intensity compared with that of strawberries [50]. The photosynthetic rate of tomato leaves was evaluated under simulated solar irradiation through the P3HT:FNTz-FA-based OSCs and compared with control conditions. By focusing on the results of the control experiment, the saturation point of the photosynthetic rate for tomato leaves in Fig. 6e is around 900 mmol/m^2/s, which corresponds to an irradiance of 450 W/m^2. As mentioned above, the saturation point of strawberry leaves based on Fig. 6b is an irradiance of 250 W/m^2. These results are in good agreement with the reported growing environments showing that tomatoes need higher light intensity to grow compared with that of strawberries [50]. As shown in Fig. 6e, the direct irradiation of simulated sunlight showed an apparent high photosynthetic rate compared with the transmission of the P3HT:FNTz-FA-based OSCs, which is thought to be due to the large influence of the difference in transmittance. To investigate the influence of the green-light wavelength-selectivity on tomato growth, we also measured the photosynthetic rate under 25% transmitted light through a natural density filter. The transmittance spectra are summarized in Fig. S11. As shown in Fig. 6e, the P3HT:FNTz-FA-based OSCs exhibited an almost comparable photosynthetic rate against the controlled 25% transmitted light conditions. These results indicate that the green-light wavelength-selective absorption has no detrimental effect on photosynthesis. However, the optimization of irradiation intensity must be considered for the cultivation of tomatoes.

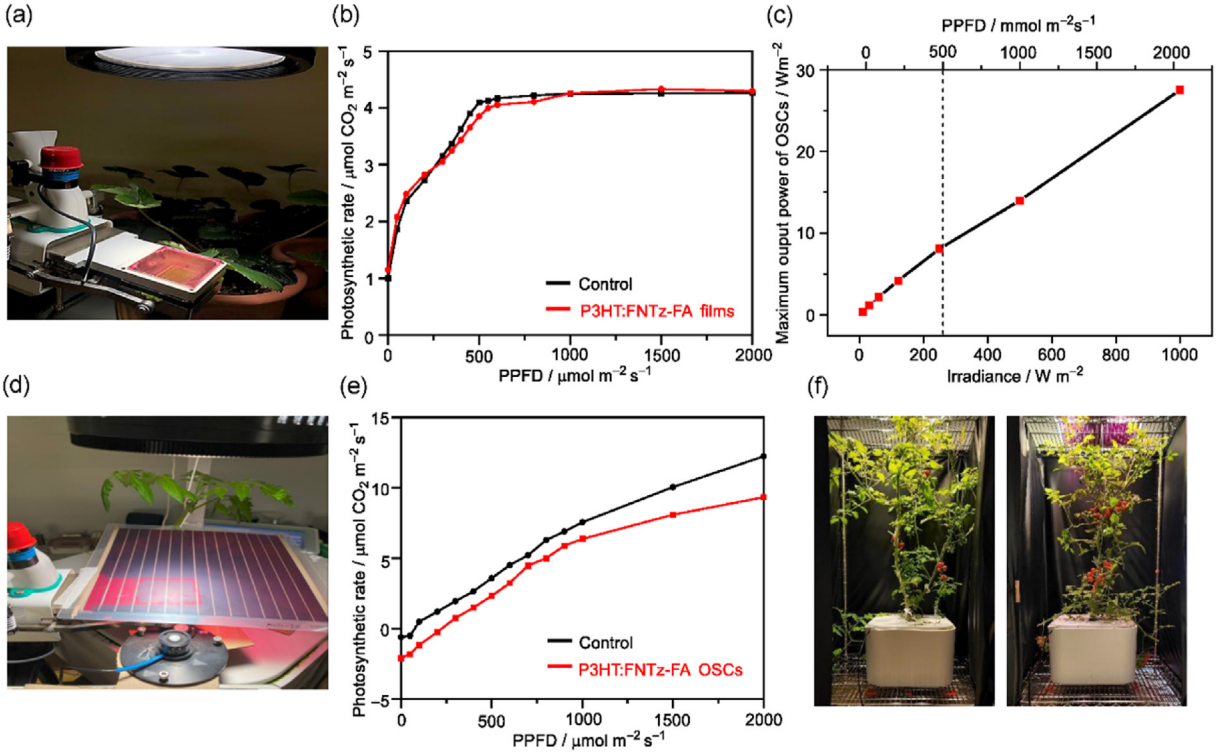

Fig. 6. (a) Photo of photosynthetic experiments with P3HT:FNTz-FA films. (b) Photosynthetic rate of strawberries under the P3HT:FNTz-FA films against PPFD. (c) Maximum output power of OSCs vs. PPFD and irradiance. (d) Photo of photosynthetic experiments with P3HT:FNTz-FA-based OSCs. (e) Photosynthetic rate of tomatoes under the P3HT:FNTz-FA-based OSCs. (f) Photos of tomato growth under control (left) and with P3HT:FNTz-FA-based OSCs (right). OSCs: organic solar cells; PPFD: photosynthetic photon flux density.

Finally, we preliminarily investigated the influence of the P3HT:FNTz-FA-based OSCs on crop growth under the irradiation of white LED light conditions. We selected tomatoes for this evaluation as a typical greenhouse crop. The growing conditions were set with a temperature range of 15−25 °C, humidity between 20% and 40%, a daily irradiation time of 12 h, and a cultivation period of 20 weeks. Two tomato plants were grown under white LED light conditions for up to 16 weeks using 8-week seedlings, and then one tomato was grown by transmitted light of P3HT:FNTz-FA-based OSCs for 20 weeks. A photograph of this measurement is shown in Fig. 6f. The photographs of weekly growth records are summarized in Figs. S12 and S13. After 20 weeks, the harvest quantities and the weight per tomato under the transmission of P3HT:FNTz-FA-based OSCs were determined to be 105 and 4.4 g, respectively, and this growing result is comparable with the control conditions (82, and 2.7 g) shown in Fig. S14. Although future detailed investigations will inevitably focus on many factors such as reproducibility, irradiation power dependence, irradiation light source, dependence on the growth stage of the seedlings, and variations in tomatoes to reveal the influence of wavelength-selective absorption on crop growth, this result implies that the P3HT:FNTz-FA-blend film has the potential for application to GLWS-OSCs.

4. Conclusions

In summary, we investigated GLWS-OSCs composed of P3HT as the donor and FNTz-FA as the acceptor and found that the combination can effectively harvest solar energy in the green-light region for electricity and transmit in the blue-light and red-light regions for crop growth. The well-matched ΔE_{opt} of FNTz-FA (2.08 eV) makes it compatible to blend with cost-effective and bulk-available P3HT (ΔE_{opt} = 1.91 eV) as the donor. The chemical structure of FNTz-FA showed superior chemical stability compared with that of the representative NFAs of ITIC and Y6. To consider the fabrication of module-sized devices, OSCs based on P3HT and FNTz-FA with an inverted configuration were optimal. Furthermore, 100 and 400 cm^2-scale OSC modules were successfully fabricated, which showed a reasonable PCE with sufficient device stability. The AVT value of the P3HT:FNTz-FA-blend films was calculated to be as high as 46%. The quantitative parameters of S_G and PCE-GR for GLWS-OSCs were determined to be 0.59 and 11.7%, respectively, and these values are higher than those of our previously reported GLWS-OSCs. Photosynthetic rate measurements revealed that the P3HT:FNTz-FA-blend film poses no interference in the growth of strawberries, and the green-light wavelength-selective absorbance shows no negative influence on the photosynthetic rate for tomatoes under the same transmitted irradiation power. The preliminary investigations of tomatoes grown under indoor conditions implied the potential of the P3HT:FNTz-FA-based OSCs for agrivoltaics. These combined results clearly demonstrate the potential of the GLWS-OSCs for agrivoltaics in greenhouses. Further studies in terms of both OSCs and agriculture are inevitable to achieve the social implementation of GLWS-OSCs. Therefore, development of NFAs with improved S_G and PCE-GR values as well as investigation into the influence of green-light wavelength-selective absorption on crop growth under solar irradiation in greenhouses are ongoing by our group.

CRediT authorship contribution statement

Shreyam Chatterjee: Writing − original draft, Conceptualization. **Naoto Shimohara:** Investigation. **Takuji Seo:** Investigation. **Seihou Jinnai:** Visualization, Investigation. **Taichi Moriyama:** Funding acquisition. **Morihiko Saida:** Investigation. **Kenji Omote:** Investigation. **Kento Hama:** Investigation. **Yohei Iimuro:** Investigation. **Yasuyuki Watanabe:** Conceptualization. **Yutaka Ie:** Writing − review & editing, Supervision, Project administration, Funding acquisition.

Declaration of competing interest

The authors declare that they have no known competing financial interests or personal relationships that could have appeared to influence the work reported in this paper.

Data availability

No data was used for the research described in the article.

Acknowledgements

This work was supported by JSPS KAKENHI (20H02814, 20H05841, 20KK0123, 23K17947, 20K15352, 23H02064, 23K04913, and 24H00482), NEDO (21500248-0), JST (JPMJMI22I1, JPMJSF23B3), JST-CREST (JPMJCR20R1), and the Mitsubishi Foundation (202310004). We acknowledge the support of AIRC center, SANKEN, Osaka University. We are thankful to Mr. Masahiro Suzuki and Mr. Syou Mochiduki for the assistance of photosynthetic rate measurements. We are also thankful to Ms. Nao Eguchi at the CAC, SANKEN for measuring ToF-SIMS.

Appendix A. Supplementary data

Supplementary data to this article can be found online at https://doi.org/10.1016/j.mtener.2024.101673.

References

[1] M. Victoria, N. Haegel, I.M. Peters, R. Sinton, A. Jäger-Waldau, C. Del Cañizo, C. Breyer, M. Stocks, A. Blakers, I. Kaizuka, K. Komoto, A. Smets, Solar photovoltaics is ready to power a sustainable future, Joule 5 (2021) 1041, https://doi.org/10.1016/j.joule.2021.03.005.
[2] P. Huang, Y. Sun, M. Lovati, X. Zhang, Solar-photovoltaic-power-sharing-based design optimization of distributed energy storage systems for performance improvements, Energy 222 (2021) 119931, https://doi.org/10.1016/j.energy.2021.11993.
[3] T. Sekiyama, A. Nagshima, Solar sharing for both food and clean energy production: performance of agrivoltaic systems for corn, a typical shade-intolerant crop, Environments 6 (2019) 65, https://doi.org/10.3390/environments6060065.
[4] S. Gorjian, J. Jamshidian, A. Gorjian, H. Faridi, M. Vafaei, F. Zhang, W. Liu, P.E. Campana, Technological advancements and research prospects of innovative concentrating agrivoltaics, Appl. Energy 337 (2023) 120799, https://doi.org/10.1016/j.apenergy.2023.120799.
[5] J. Li, H.-L. Cao, W.-B. Jiao, Q. Wang, M. Wei, I. Cantone, J. Lü, A. Abate, Biological impact of lead from halide perovskites reveals the risk of introducing a safe threshold, Nat. Commun. 11 (2020) 310, https://doi.org/10.1038/s41467-019-13910-y, 2020.
[6] P. Su, Y. Liu, J. Zhang, C. Chen, B. Yang, C. Zhang, X. Zhao, Pb-based perovskite solar cells and the underlying pollution behind clean energy: dynamic leaching of toxic substances from discarded perovskite solar cells, J. Phys. Chem. Lett. 11 (2020) 2812, https://doi.org/10.1021/acs.jpclett.0c00503.
[7] D. Luo, W. Jang, D.D. Babu, M.S. Kim, D.H. Wang, Recent progress in organic solar cells based on non-fullerene acceptors: materials to devices, J. Mater. Chem. A 10 (2022) 3255, https://doi.org/10.1039/d1ta10707k.
[8] K. Inada, Action spectra for photosynthesis in higher plants, Plant Cell Physiol. 17 (1976) 355, https://doi.org/10.1093/oxfordjournals.pcp.a075288.
[9] S. Jinnai, A. Oi, T. Seo, T. Moriyama, M. Terashima, M. Suzuki, Ken-Ichi Nakayama, Y. Watanabe, Y. Ie, Green-light wavelength-selective organic solar cells based on poly(3-hexylthiophene) and naphthobisthiadiazole-containing acceptors toward agrivoltaics, ACS Sustain. Chem. Eng. 11 (2023) 1548, https://doi.org/10.1021/acssuschemeng.2c06426.
[10] C.J.M. Emmott, J.A. Röhr, M. Campoy-Quiles, T. Kirchartz, A. Urbina, N.J. Ekins-Daukes, J. Nelson, Organic photovoltaic greenhouses: a unique application for semi-transparent PV? Energy Environ. Sci. 8 (2015) 1317, https://doi.org/10.1039/c4ee03132f.
[11] F. Yang, Y. Zhang, Y. Hao, Y. Cui, W. Wang, T. Ji, F. Shi, B. Wei, Visibly transparent organic photovoltaic with improved transparency and absorption based on tandem photonic crystal for greenhouse application, Appl. Opt. 54 (2015) 10232, https://doi.org/10.1364/AO.54.010232.

[12] C.S. Allardyce, C. Fankhauser, S.M. Zakeeruddin, M. Grätzel, P.J. Dyson, The influence of greenhouse-integrated photovoltaics on crop production, Sol. Energy 155 (2017) 517, https://doi.org/10.1016/j.solener.2017.06.044.
[13] H. Shi, R. Xia, G. Zhang, H.-L. Yip, Y. Cao, Spectral engineering of semi-transparent polymer solar cells for greenhouse applications, Adv. Energy Mater. 9 (2019) 1803438, https://doi.org/10.1002/aenm.201803438.
[14] Y. Liu, P. Cheng, T. Li, R. Wang, Y. Li, S.-Y. Chang, Y. Zhu, H.-W. Cheng, K.-H. Wei, X. Zhan, B. Sun, Y. Yang, Unraveling sunlight by transparent organic semiconductors toward photovoltaic and photosynthesis, ACS Nano 13 (2019) 1071, https://doi.org/10.1021/acsnano.8b08577.
[15] Y. Zhao, Y. Zhu, H.-W. Cheng, R. Zheng, D. Meng, Y. Yang, A review on semi-transparent solar cells for agricultural application, Mater. Today Energy 22 (2021) 100852, https://doi.org/10.1016/j.mtener.2021.100852.
[16] D.A. Chalkias, E. Stathatos, The Emergence of Agrivoltaics: Current Status, Challenges and Future Opportunities, Green Energy and Technology, Springer Nature Switzerland, Springer Cham, 2024, https://doi.org/10.1007/978-3-031-48861-0.
[17] D. Xie, Y. Zhang, X. Yuan, Y. Li, F. Huang, Y. Cao, C. Duan, A 2.20 eV bandgap polymer donor for efficient colorful semitransparent organic solar cells, Adv. Funct. Mater. 33 (2023) 2212601, https://doi.org/10.1002/adfm.202212601.
[18] S. Jinnai, Y. Ie, M. Karakawa, T. Aernouts, Y. Nakajima, S. Mori, Y. Aso, Electron-accepting π-conjugated systems for organic photovoltaics: influence of structural modification on molecular orientation at donor−acceptor interfaces, Chem. Mater. 28 (2016) 1705, https://doi.org/10.1021/acs.chemmater.5b04551.
[19] S. Chatterjee, Y. Ie, M. Karakawa, Y. Aso, Naphtho[1,2-*c*:5,6-*c*']bis[1,2,5]thiadiazole-containing π-conjugated compound: nonfullerene electron acceptor for organic photovoltaics, Adv. Funct. Mater. 29 (2016) 1161, https://doi.org/10.1002/adfm.201504153.
[20] S. Holliday, R.S. Ashraf, A. Wadsworth, D. Baran, S.A. Yousaf, C.B. Nielsen, C.-H. Tan, S.D. Dimitrov, Z. Shang, N. Gasparini, M. Alamoudi, F. Laquai, C.J. Brabec, A. Salleo, J.R. Durrant, I. McCulloch, High-efficiency and air-stable P3HT-based polymer solar cells with a new non-fullerene acceptor, Nat. Commun. 7 (2016) 11585, https://doi.org/10.1038/ncomms11585.
[21] S. Chatterjee, T. Ohto, H. Tada, S. Jinnai, Y. Ie, Correlation between the dipole moment of nonfullerene acceptors and the active layer morphology of green-solvent-processed P3HT-based organic solar cells, ACS Sustain. Chem. Eng. 8 (2020) 19013, https://doi.org/10.1021/acssuschemeng.0c07114.
[22] C. Yang, S. Zhang, J. Ren, M. Gao, P. Bi, L. Ye, J. Hou, Molecular design of a non-fullerene acceptor enables a P3HT-based organic solar cell with 9.46% efficiency, Energy Environ. Sci. 13 (2020) 2864, https://doi.org/10.1039/d0ee01763a.
[23] S. Chatterjee, S. Jinnai, Y. Ie, Nonfullerene acceptors for P3HT-based organic solar cells, J. Mater. Chem. A 9 (2021) 18857, https://doi.org/10.1039/d1ta03219d.
[24] S. Chatterjee, Y. Ie, Synthesis, properties, and photovoltaic characteristics of fluoranthenedione-containing nonfullrene acceptors for organic solar cells, J. Photopolym, Sci. Technol. 35 (2022) 187, https://doi.org/10.2494/photopolymer.35.187.
[25] S. Jinnai, N. Shimohara, K. Ishikawa, T. Washio, Y. Watanabe, Y. Ie, Green-light wavelength-selective organic solar cells for agrivoltaics: dependence of wavelength on photosynthetic rate, Faraday Discuss 250 (2024) 220, https://doi.org/10.1039/D3FD00141E.
[26] S. Chatterjee, Y. Ie, T. Seo, T. Moriyama, G.-J.A.H. Wetzelaer, P.W.M. Blom, Y. Aso, Fluorinated naphtho[1,2-*c*:5,6-*c*']bis[1,2,5] thiadiazole-containing π-conjugated compound: synthesis, properties, and acceptor applications in organic solar cells, NPG Asia Mater. 10 (2018) 1016, https://doi.org/10.1038/s41427-018-0088-4.
[27] H.I. Gonev, E. Jones, C.-Y. Chang, Y. Ie, S. Chatterjee, T.M. Clarke, Invariant charge carrier dynamics using a non-planar non-fullerene acceptor across multiple processing solvents, J. Phys. Chem. C 128 (2024) 6758, https://doi.org/10.1021/acs.jpcc.4c00708.
[28] M. Vezie, S. Few, I. Meager, Exploring the origin of high optical absorption in conjugated polymers, Nat. Mater. 15 (2016) 746, https://doi.org/10.1038/nmat4645.
[29] M. Jørgensen, K. Norrman, S.A. Gevorgyan, T. Tromholt, B. Andreasen, F.C. Krebs, Stability of polymer solar cells, Adv. Mater. 24 (2012) 580, https://doi.org/10.1002/adma.201104187.
[30] M. Manceau, S. Chambon, A. Rivaton, J.-L. Gardette, S. Guillerez, N. Lemaître, Effects of long-term UV−visible light irradiation in the absence of oxygen on P3HT and P3HT:PCBM blend, Sol. Energy Mater. Sol. Cells 94 (2010) 1572, https://doi.org/10.1016/j.solmat.2010.03.012.
[31] W. Li, D. Liu, T. Wang, Stability of non-fullerene electron acceptors and their photovoltaic devices, Adv. Funct. Mater. 31 (2021) 2104552, https://doi.org/10.1002/adfm.202104552.
[32] X. Zhu, L. Hu, W. Wang, X. Jiang, L. Hu, Y. Zhou, Reversible chemical reactivity of non-fullerene acceptors for organic solar cells under acidic and basic environment, ACS Appl. Energy Mater. 2 (2019) 7602, https://doi.org/10.1021/acsaem.9b01591.
[33] P. Jiang, L. Hu, L. Sun, Z. Li, H. Han, Y. Zhou, On the interface reactions and stability of nonfullerene organic solar cells, Chem. Sci. 13 (2022) 4714, https://doi.org/10.1039/d1sc07269b.
[34] Y. Zhou, C. Fuentes-Hernandez, J. Shim, J. Meyer, A.J. Giordano, H. Li, P. Winget, T. Papadopoulos, H. Cheun, J. Kim, M. Fenoll, A. Dindar, W. Haske, E. Najafabadi, T.M. Khan, H. Sojoudi, S. Barlow, S. Graham, J.-L. Bredas, S.R. Marder, A. Kahn, B. Kippelen, A universal method to produce low−work function electrodes for organic electronics, Science 336 (2012) 327, https://doi.org/10.1126/science.1218829.
[35] H. Kang, S. Hong, J. Lee, K. Lee, Electrostatically self-assembled nonconjugated polyelectrolytes as an ideal interfacial layer for inverted polymer solar cells, Adv. Mater. 24 (2012) 3005, https://doi.org/10.1002/adma.201200594.
[36] L. Hu, S. Xiong, W. Wang, L. Sun, F. Qin, Y. Zhou, Influence of substituent groups on chemical reactivity kinetics of nonfullerene acceptors, J. Phys. Chem. C 124 (2020) 2307, https://doi.org/10.1021/acs.jpcc.9b09833.
[37] J. Cameron, P.J. Skabara, The damaging effects of the acidity in PEDOT:PSS on semiconductor device performance and solutions based on non-acidic alternatives, Mater. Horiz. 7 (2020) 1759, https://doi.org/10.1039/c9mh01978b.
[38] M.P. de Jong, L.J. van Ijzendoorn, M.J.A. de Voigt, Stability of the interface between indium-tin-oxide and poly(3,4-ethylenedioxythiophene)/poly(-styrenesulfonate) in polymer light-emitting diodes, Appl. Phys. Lett. 77 (2000) 2255, https://doi.org/10.1063/1.1315344.
[39] F.J. Lim, K. Ananthanarayanan, J. Luther, G.W. Ho, Influence of a novel fluorosurfactant modified PEDOT:PSS hole transport layer on the performance of inverted organic solar cells, J. Mater. Chem. 22 (2012) 25057, https://doi.org/10.1039/c2jm35646e.
[40] C. Waldauf, M. Morana, P. Denk, P. Schilinsky, K. Coakley, S. Choulis, C. Brabec, Highly efficient inverted organic photovoltaics using solution based titanium oxide as electron selective contact, Appl. Phys. Lett. 89 (2006) 233517, https://doi.org/10.1063/1.2402890.
[41] H. Sun, J. Weickert, H.C. Hesse, L. Schmidt-Mende, UV light protection through TiO_2 blocking layers for inverted organic solar cells, Sol. Energy Mater. Sol. Cells 95 (2011) 3450, https://doi.org/10.1016/j.solmat.2011.08.004.
[42] Z. Liang, Q. Zhang, O. Wiranwetchayan, J. Xi, Z. Yang, K. Park, C. Li, G. Cao, Effects of the morphology of a ZnO buffer layer on the photovoltaic performance of inverted polymer solar cells, Adv. Funct. Mater. 22 (2012) 2194, https://doi.org/10.1002/adfm.201101915.
[43] M. Finšgar, Tandem GCIB-ToF-SIMS and GCIB-XPS analyses of the 2-mercaptobenzothiazole on brass, npj Mater. Degrad. 7 (2023) 1, https://doi.org/10.1038/s41529-022-00317-2.
[44] S. Strohm, F. Machui, S. Langner, P. Kubis, N. Gasparini, M. Salvador, I. McCulloch, H.-J. Egelhaaf, C.J. Brabec, P3HT: non-fullerene acceptor based large area, semi-transparent PV modules with power conversion efficiencies of 5%, processed by industrially scalable methods, Energy Environ. Sci. 11 (2018) 2225, https://doi.org/10.1039/c8ee01150h.
[45] ASTM G173-03, Standard Tables for Reference Solar Spectral Irradiances: Direct Normal and Hemispherical on 37° Tilted Surface, ASTM International, Pennsylvania, USA, 2012, https://doi.org/10.1520/G0173-03R12.
[46] C.J. Traverse, R. Panday, M.C. Barr, R.R. Lunt, Emergence of highly transparent photovoltaics for distributed applications, Nat. Energy 2 (2017) 849, https://doi.org/10.1038/s41560-017-0016-9.
[47] K.-S. Chen, J.-F. Salinas, H.-L. Yip, L. Huo, J. Hou, A.K.-Y. Jen, Semi-transparent polymer solar cells with 6% PCE, 25% average visible transmittance and a color rendering index close to 100 for power generating window applications, Energy Environ. Sci. 5 (2012) 9551, https://doi.org/10.1039/c2ee22623e.
[48] M.E. Loik, S.A. Carter, G. Alers, C.E. Wade, D. Shugar, C. Corrado, D. Jokerst, C. Kitayama, Wavelength-selective solar photovoltaic systems: powering greenhouses for plant growth at the food-energy-water nexus, Earth's Future 5 (2017) 1044, https://doi.org/10.1002/2016EF000531.
[49] J. Liu, W. Iersel, Photosynthetic physiology of blue, green, and red light: light intensity effects and underlying mechanisms, Front. Plant Sci. 12 (2021) 619987, https://doi.org/10.3389/fpls.2021.619987.
[50] K. Maeda, Y. Ito, Effect of different PPFDs and photoperiods on growth and yield of everbearing strawberry 'Elan' in plant factory with white LED lighting, Environ. Control Biol. 58 (2020) 99, https://doi.org/10.2525/ecb.58.99.